Multimodal Distribution of Quantum Confinement in Ripened CdSe Nanocrystals

Dino Tonti,*[,†,‡] Mona B. Mohammed,[†,§] Awos Al-Salman,[†] Philip Pattison,[||] and Majed Chergui[†]

Laboratoire de Spectroscopie Ultrarapide, Ecole Polytechnique Fédérale de Lausanne, ISIC, FSB, BSP CH-1015 Lausanne, Switzerland, and Laboratoire de Cristallographie, Ecole Polytechnique Fédérale de Lausanne, IPMC, FSB, BSP CH-1015 Lausanne, Switzerland

Received May 28, 2007. Revised Manuscript Received November 7, 2007

We present three different preparation methods for CdSe colloidal nanoparticles that, when carried out into the Ostwald ripening regime, lead to the development of complex spectral patterns resulting from the overlap of several distinct components corresponding to different kinds of nanoparticles coexisting in solution. Although several polyhedral shapes are present in the transmission electron microscopy images, the main spectral difference appears to be essentially due to different sizes. We explain the generation of different species with a mechanism implying a controlled etching of the initially spherical particles and their subsequent coalescence into larger particles. We suggest that the presence of water and oxygen in the chemical equilibria may favor this process.

Introduction

Growth of colloidal inorganic nanoparticles in organic amphiphilic media (i.e., lipophilic and/or surfactant molecules) has achieved excellent levels of size and shape homogeneity in the past years.[1–3] After a rapid nucleation step, the growth process is usually considered to occur in two stages. In the first, which we call reactive growth, all crystals grow in parallel by precipitation of the elements coming from the decomposition of either the precursor complexes or small unstable clusters. When the precursors in solution are exhausted, a competition among relatively stable particles starts, and growth enters the second stage. The elemental species of the crystals will be exchanged among the particles to the advantage of those having lower energy, that is, the largest ones. This mechanism, known as coarsening or Ostwald ripening, leads to a broadening of the size distribution, as larger particles will grow while smaller ones shrink.[4–7] Conversely, growth conditions for optimal particle synthesis are able to give a smaller growth rate to larger particles during the initial stage of growth from the precursors. Peng et al.,[8] who first reported a narrowing and then a broadening of the size distribution in the course of the growth, referred to the two stages as "focusing" and "defocusing".

While most efforts have obviously been directed to find conditions for the sharpest focusing, fewer studies have reported on the Ostwald ripening in organic media. Mathematical models predict that Ostwald ripening does not necessarily lead to a poorer sample, at least in cases where the starting size distribution is already broad.[6,7] A number of reports suggest that actually another growth process is possible during Ostwald ripening: particle coalescence by aggregation[9] or oriented attachment.[10–15] Different possible causes have been invoked: ligand depletion or particle self-assembly due to, for example, electrostatic fields induced by a permanent dipole[14] or just particle collision in solution.[16] In a few cases it is rather simple to prove a coalescence mechanism if the shape of the building block can be recognized in the final shape of the obtained object (such as rod, wire, multipod, ring)[14] or in the arrangement of the lattice defects.[10] If atomic rearrangement follows oriented attachment of any sort of fusion mechanism, it is more difficult to find evidence. For this reason, such "non-classical

* Corresponding author. Phone: +34-913349026. Fax: +34-913720623. E-mail: dino@icmm.csic.es.
† Laboratoire de Spectroscopie Ultrarapide.
‡ Current address: Instituto de Ciencia de Materiales de Madrid, CSIC, c/Sor Juana Inès de la Cruz, 3, 28049 Madrid, Spain.
§ Current address: National Institute of Laser Enhanced Sciences (NILES), Cairo University, Egypt.
|| Laboratoire de Cristallographie.

(1) Talapin, D. V.; Rogach, A. L.; Kornowski, A.; Haase, M.; Weller, H. *Nano Lett.* **2001**, *1*, 207.
(2) Yu, W. W.; Falkner, J. C.; Shih, B. S.; Colvin, V. L. *Chem. Mater.* **2004**, *16*, 3318.
(3) Donega, C. D.; Liljeroth, P.; Vanmaekelbergh, D. *Small* **2005**, *1*, 1152.
(4) Wagner, C. *Z. Elektrochem.* **1961**, *65*, 581.
(5) Lifshitz, I. M.; Slyozov, V. V. *J. Phys. Chem. Solids* **1961**, *19*, 35.
(6) Talapin, D. V.; Rogach, A. L.; Haase, M.; Weller, H. *J. Phys. Chem. B* **2001**, *105*, 12278.
(7) Mantzaris, N. V. *Chem. Eng. Sci.* **2005**, *60*, 4749.
(8) Peng, X. G.; Wickham, J.; Alivisatos, A. P. *J. Am. Chem. Soc.* **1998**, *120*, 5343.
(9) Ocana, M.; Rodriguez Clemente, R.; Serna, C. J. *Adv. Mater.* **1995**, *7*, 212.
(10) Penn, R. L.; Banfield, J. F. *Science* **1998**, *281*, 969.
(11) Penn, R. L.; Oskam, G.; Strathmann, T. J.; Searson, P. C.; Stone, A. T.; Veblen, D. R. *J. Phys. Chem. B* **2001**, *105*, 2177.
(12) Huang, F.; Zhang, H. Z.; Banfield, J. F. *Nano Lett.* **2003**, *3*, 373.
(13) Ribeiro, C.; Lee, E. J. H.; Giraldi, T. R.; Longo, E.; Varela, J. A.; Leite, E. R. *J. Phys. Chem. B* **2004**, *108*, 15612.
(14) Cho, K. S.; Talapin, D. V.; Gaschler, W.; Murray, C. B. *J. Am. Chem. Soc.* **2005**, *127*, 7140.
(15) Niederberger, M.; Colfen, H. *Phys. Chem. Chem. Phys.* **2006**, *8*, 3271.
(16) Ribeiro, C.; Lee, E. J. H.; Longo, E.; Leite, E. R. *ChemPhysChem* **2005**, *6*, 690.

10.1021/cm071439u CCC: $40.75
Published on Web 01/23/2008

crystal growth mechanisms" involving mesoscale transformations might be more common than usually considered.[15]

For hydrothermal growth of ZnS in concentrated NaOH[17] or thiol-capped PbS,[18] Zhang et al. found that the best fit of the kinetics implies an oriented attachment mechanism of small clusters; they observed a two-stage process, where first oriented attachment only occurs and then oriented attachment and Ostwald ripening compete. They speculate that this scheme may be general. In fact, with oriented attachment the expected growth rate is larger for smaller particles (which implies focusing) while in the Ostwald ripening regime larger particles are favored; thus, defocusing is observed.[18] They found that strongly attached ligands retaining ions from dissolution delay the rate of Ostwald ripening while they do not affect the oriented attachment.

In this work we show that complex equilibria during Ostwald ripening, at the end of the colloidal synthesis of CdSe nanocrystals (NCs) at high temperature, can lead to the selection of certain sizes and nonspherical shapes, which eventually appear as distinct components in optical spectra.

We observed this event in three different synthesis procedures that we implemented: (I) our preparation of zinc blende (ZB) NCs, using phosphonic acids added to the Se source,[19] (II) Cao et al.'s one-pot synthesis of ZB CdSe, where they used elemental Se,[20] and (III) a standard wurtzite (W) CdSe preparation, where we used a hydrated Cd source.

In all cases, we clearly observe the emergence of several components in absorption and photoluminescence (PL) spectra, while in transmission electron microscopy (TEM) we often recognize well-defined faceted geometrical shapes of different sizes. This indicates that in all these cases Ostwald ripening leads to multimodal distributions of the particle quantum confinement as a result of the presence of several characteristic sizes and/or shapes.

Facets in colloidal nanoparticles prepared in amphiphilic media have been previously reported by other authors. Cao et al. observed tetrahedral particles with their preparation of ZB CdSe when they used tributylphosphine selenide instead of selenium, which is less reactive.[20] However, they did not comment on the mechanism of formation of such a shape, and it is not clear whether this was obtained by a kinetically controlled growth or through a ripening process. Li et al. have found that a mild chemical etching process can select CdSe NCs with faceted shapes, which show superior luminescence and stability to further etching.[21] Peng et al. controlled the reversible formation of ZnO nanopyramids by switching on and off Ostwald ripening through addition of fatty acids and methanol.[22]

Kudera et al. have recently reported the optical spectra of the sequential formation of magic-sized CdSe clusters in mild synthesis conditions;[23] however, we are not aware of any report of optical spectra evolution corresponding to a size and shape selection during the Ostwald ripening stage of the growth in an amphiphilic medium. We will attempt to relate our chemical conditions with possible nonclassical growth mechanisms.

Experimental Section

All materials were used as received without further purification: cadmium oxide (CdO, Fluka, 99%), cadmium acetate dihydrate (Riedel, 99%), selenium powder (Riedel, 99%), oleic acid (Aldrich, 90%), stearic acid (Fluka, 98.5%), trioctylphosphine (TOP, Fluka, 90%), 1-octadecene (ODE, Fluka, 95%), octadecylamine (ODA, Aldrich, 97%), hexadecylamine (HDA, Aldrich, 97%), tetradecylphosphonic acid (TDPA, Alfa, 97%), and trioctylphosphine oxide (TOPO, Alfa, 97%).

A first method (hereafter, called method I) to prepare CdSe nanoparticles with a ZB lattice structure was described earlier.[19] Briefly, 0.25 g of CdO were dissolved in 2 g of oleic acid and 6 mL of ODE and brought to a temperature of 240 °C. A Se solution (0.2 g of Se powder, 3 mL of TOP, 3 g of ODA, and 2 g of TDPA, heated until melt) was then injected into the reaction flask. The temperature was adjusted to a value of 240 °C throughout the course of the growth.

The second method (II) was based on the approach without injection published by Cao et al.[20] A 46 mg portion of CdO was added to 0.55 g of oleic acid and 20 g of ODE, heated to 160 °C until the solution became clear, and then cooled down. Then, 22 mg of Se powder was added and the temperature increased at a rate of 25 °C/min until 220 °C, when a further 9 g of oleic acid was added. Finally, the temperature was increased to 290 °C.

The last method (III) was a hot injection synthesis in TOPO. A 0.10 g quantity of Cd acetate dihydrate was added with 2 g of stearic acid and 5 g of TOPO and brought to a temperature of 295 °C. A 0.22 g quantity of Se was dissolved in 8 mL of TOP and injected into the reaction flask. During growth, the temperature was allowed to rise again to 280 °C.

In all cases, the Cd solution was heated under nitrogen. To follow the reaction during the growth process, aliquots of the mixture were removed from the reaction flask at regular time intervals and dissolved in toluene. To isolate the CdSe NCs from the organic subproducts and from unreacted materials, the sample was precipitated with a 3:3:1 methanol/acetone/chloroform mixture and redissolved in toluene.

TEM images were obtained with a Philips CM20 microscope, operating at an accelerating voltage of 200 kV. A drop from a very dilute sample solution was deposited on an amorphous carbon−copper grid and left to evaporate at room temperature.

For X-ray diffraction (XRD) measurements, the samples were precipitated with methanol from the washed toluene solution and allowed to dry in air. Synchrotron-radiation based diffraction (SXRD) data were collected at the Swiss-Norwegian beam line, ESRF, Grenoble, using the MAR345 image plate area detector at room temperature. The sample mount was a glass fiber needle with about 1 mm^3 of material mounted on the end of the needle. Data were collected at a wavelength of 0.71 Å, with an exposure time

(17) Zhang, J.; Lin, Z.; Lan, Y. Z.; Ren, G. Q.; Chen, D. G.; Huang, F.; Hong, M. C. *J. Am. Chem. Soc.* **2006**, *128*, 12981.
(18) Zhang, J.; Wang, Y. H.; Zheng, J. S.; Huang, F.; Chen, D. G.; Lan, Y. Z.; Ren, G. Q.; Lin, Z.; Wang, C. *J. Phys. Chem. B* **2007**, *111*, 1449.
(19) Mohamed, M.; Tonti, D.; Al Salman, A.; Chemseddine, A.; Chergui, M. *J. Phys. Chem. B* **2005**, *109*, 1533.
(20) Yang, Y. A.; Wu, H. M.; Williams, K. R.; Cao, Y. C. *Angew. Chem., Int. Ed.* **2005**, *44*, 6712.
(21) Li, R. F.; Lee, J.; Yang, B. C.; Horspool, D. N.; Aindow, M.; Papadimitrakopoulos, F. *J. Am. Chem. Soc.* **2005**, *127*, 2524.
(22) Chen, Y.; Kim, M.; Lian, G.; Johnson, M. B.; Peng, X. *J. Am. Chem. Soc.* **2005**, *127*, 13331.
(23) Kudera, S.; Zanella, M.; Giannini, C.; Rizzo, A.; Li, Y. Q.; Gigli, G.; Cingolani, R.; Ciccarella, G.; Spahl, W.; Parak, W. J.; Manna, L. *Adv. Mater.* **2007**, *19*, 548.

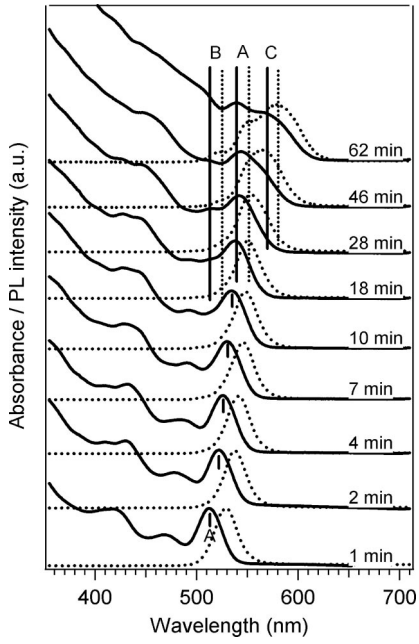

Figure 1. Extended temporal evolution of the growth of CdSe NCs prepared according to method I. Absorption (continuous lines) and emission (dotted lines) spectra have been normalized.

of 60 s per frame. Integration of the area detector images was made using the FIT2D software.

For the absorption and luminescence measurements, the sample was dispersed in 10 mm fluorescence cuvettes filled with toluene. An Avantes AvaSpec-2048 Fiber Optic spectrometer was used for both absorption and PL measurements. The excitation source was a 20 W halogen lamp for the absorption and a 100 mW Luxeon royal blue light emitting diode (max emission at 450 nm) for the PL. PL excitation (PLE) spectra were measured in an SPEX Fluorolog 2 system, using a Thermo-Oriel 150 W tungsten lamp as the excitation source, which was also used for the PL measurements. Absorption spectra in the same figures were recorded with a Perkin-Elmer Lambda 35 spectrometer. In situ absorbance was recorded using a homemade dip probe connected via a Y optic fiber cable to the spectrometer and to the halogen lamp. The probed optical path could be adjusted and was typically of the order of 0.1 mm.

Results and Discussion

In the following, we first present the three preparations where we observed unusual absorption and emission spectra; then, we show that the new components belong to well-defined species; and finally, we discuss their genesis and possible chemical causes.

Preparation Method I. Our method of producing rather large ZB NCs[19] leads to a sharp distribution of sizes, allowing a clear separation of the absorption bands. In particular, we found that the splitting between the lowest two absorption bands is ∼50% larger than in W dots.

When carried out over a longer time, into the ripening regime, our method leads to the appearance of multiple components in the optical spectra. This is shown in Figure 1, with absorption and emission spectra of sample aliquots taken over a longer time. The fast red shift of the first absorption maximum ceases when it reaches a position around 530 nm. This marks the end of the focused growth and the beginning of the Ostwald ripening.[8] After this point one usually expects a broadening of all absorption and emission bands. Instead, in Figure 1 we clearly distinguish new bands that develop simultaneously in both absorption and emission spectra. This is a clear sign that distinct types of CdSe nanoparticles develop from the initial nearly monodisperse ensemble.

Indeed, at the earlier times we recognize a single component ZB absorption spectrum, which we label A at the position of its lowest exciton band. The next band is at about 40 nm to the blue side of the first band. During the first 10 min, the evolution is as described in our previous work:[19] the A band and the emission band shift to the red. At $t \geq 18$ min, a shoulder appears at 513 nm (labeled B), between the two first absorption bands. It becomes clearer in the following spectra, where it even masks the second absorption band of the previous spectra. In addition, the first absorption band broadens remarkably. This is also the case with the corresponding emission band: its width, which before was in the 25–28 nm range, increases to ∼34 nm. A shoulder becomes evident on its red side, at ∼523 nm. If we take the Stokes shift into account, this feature indicates that band B in absorption is the first band of a new species and not the second band of a single component spectrum. This assignment rules out a phase change to W dots, which might be suggested by the small splitting and the characteristic intensity ratio between the first two visible absorption bands.

Finally, after 46 min, a third component (labeled C) appears at the red side of band B, at ∼568 nm. Emission has become asymmetric, even broader, and the shoulder on the blue side more pronounced. While the maximum has shifted red, the shoulder remains in the same spectral region. The asymmetry is justified by the contribution of components A and C to the broad emission peak. These are much clearer in the following spectrum, at 62 min, where the separation is larger and C has become more intense. Also, component A has become a distinct peak. Possibly a further component develops beyond C, but with longer heating, the bands eventually smear out, indicating a more classical ripening regime leading to a broader size distribution.

In summary, at least two new species are observed during the slow ripening process, first at the blue (B) and then at the red side (C) of the initial component (A). Comparing ripened samples of different batches prepared by this method, we found the same qualitative evolution, although the ratios and the energy of the features do not always exactly match the same positions.

Preparation Method II. We also observed new components with the ZB preparation based on the approach of Cao et al.[20] In this case we could increase the temperature above 310 °C without observing any change for at least tens of minutes. However, after times longer than 1 h, the spectra started to change as in an Ostwald ripening, with a marked broadening. The broadening eventually developed into distinct peaks, resulting in patterns similar to those obtained with method I, although the new peaks were not as sharp (see Figure 2). We always end with two clear components, whose weight depends on starting conditions and heating.

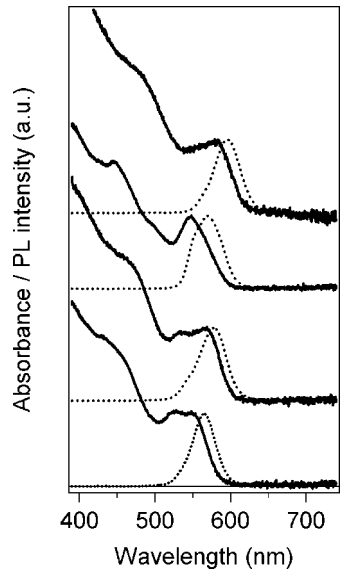

Figure 2. Absorption (continuous lines) and emission (dotted lines) spectra from four different samples prepared according to method II after ripening.

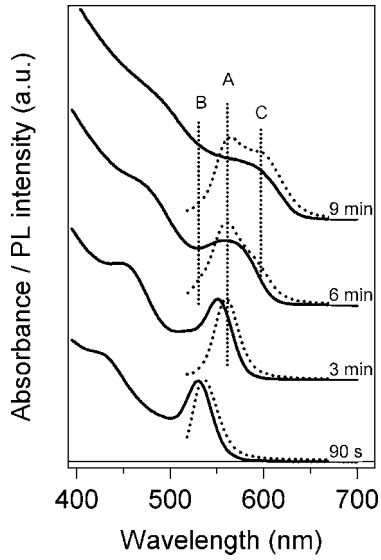

Figure 3. Temporal evolution of the growth of CdSe NCs prepared according to method III.

Their assignments and the mechanism of formation are discussed below.

Preparation Method III. Finally, we also found multiple components in a third case, when we used Cd acetate dihydrate as the Cd source, in a synthesis in TOPO without HDA. In Figure 3 we show a spectral series from this preparation. Broadening was fast and even larger than in method II: in absorption, already after 6 min, features cannot be well recognized. In emission instead, we see that a foot (B) and a shoulder (C) have developed, respectively, at the blue and at the red side of the main peak (A). Later, we see that the red component C grows while the blue one B decreases.

Thus, it appears that also in this case, when we expect Ostwald ripening, well-defined species form sequentially, first with a higher energy band and then with a lower one.

Nature of the Components. To show that the above spectra result from the overlap of signals from different

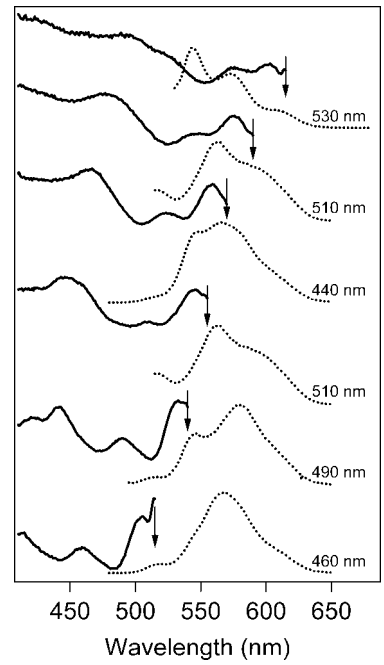

Figure 4. Set of PLE (continuous lines) and PL (dotted lines) spectra taken with different emission (PLE) or excitation (PL) wavelengths on the same ripened sample. Arrows indicate, for each excitation spectrum, the emission wavelength at which it was recorded. Depending on the excitation wavelength, different bands can be appreciated in the PL spectra. Next to each PLE, we placed the PL spectrum that best shows the closest component to the PLE emission (arrow) wavelength. Each PL spectrum has been labeled with the corresponding excitation wavelength. This arrangement is useful to compare the absorption spectrum of the different species that appear in the emission spectra.

Table 1. Emission Components Revealed in PL Spectra Taken at Different Excitation Wavelengths

	$\lambda_{excitation}$ (nm)				
$\lambda_{emission}$ (nm)	440	460	490	510	530
515 (component B)	X	X	X		
545 (component A)	X		X		X
565 (component C)	X	X		X	
575			X		X
595				X	
610	X				X

distinct species, we recorded PL spectra by exciting at different wavelengths and recorded PLE spectra at different emission wavelengths (Figure 4). The PL spectra depend strongly on the excitation wavelengths. Because different particles have similar absorption at short wavelengths, the emission with a high-energy excitation (<460 nm) is collected from all species, as is the case of PL in Figure 1. Differences in absorption are more significant at larger wavelengths; therefore, low energy excitations in Figure 4 help to reveal components on the red side of the maximum. The components A, B, and C previously seen are close to the first three components found in this sample. With excitations of lower energy, we find further three components on the red side. Table 1 summarizes the components detected for each excitation wavelength.

PLE allows the absorption measurement of species selected by their emission wavelength. Spectra taken at different emissions reveal remarkably distinct species. The splitting between the first two absorption bands is slightly larger for spectra taken at the emissions of components A and B than

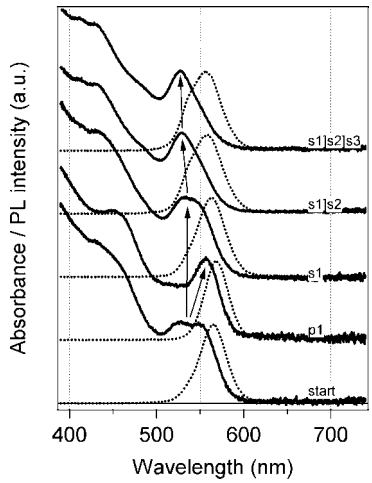

Figure 5. Absorption and emission spectra of size-selective precipitated fractions of a ripened sample from method II. Labels indicate the sequence of preparation. We use s for supernatant, p for precipitate, and the number for the separation step or generation. From the bottom sample in toluene (start), the next one comes from the part precipitated after adding methanol (p1); the following spectra (s1, s1]s2, s1]s2]s3) are three generations of the remaining supernatant after precipitation by methanol. Note that in this case the blue component has a comparatively much weaker emission than the red one. In s1]s2]s3, although the blue component dominates in absorption (and thus in the sample), in emission the red component still has a stronger peak.

for that of the more red-shifted components. Apart from this aspect, the different species do not differ considerably in their band patterns (relative positions and intensities). From different geometries we would instead expect dramatically different patterns, given the different distributions of levels and degeneracies imposed by the quantum boxes of different shapes.[24]

In an attempt to further distinguish the main constituents of the mixture, we carried out a size-selective precipitation. This technique is able to separate particles on the basis of the different tendencies to form aggregates when a nonsolvent is added. If the shape is the same, the first to precipitate are the largest particles; however, for different shapes the surface extension could play a more important role. In the present case, we added methanol to a chloroform solution of the mixture. Indeed, we observed that it is quite easy to precipitate out the red-shifted component as shown in Figure 5. By repeating the process several times, eventually the short wavelength component dominates the absorption of the more soluble supernatant fraction. This confirms that the different spectral components are indeed different species of CdSe. Those with a wider bandgap (or a higher energetic absorption edge) are the most stable in solution, a fact suggesting that the species are different in size.

TEM images of early ZB samples showed nicely spherical dots.[19,20] Ripened samples are shown in Figure 6. They are instead rather faceted, with mainly tetrahedral but also some cubic shapes. Indeed, different sizes are present. Images of two different fractions selected by addition of methanol are reported in the Supporting Information (S1) and show that those species with a higher energy band edge are actually smaller. This qualitative correlation between band edge and

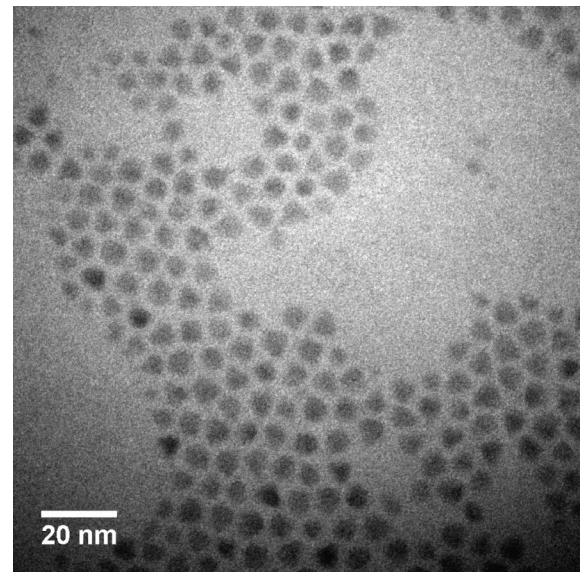

Figure 6. TEM image of a ripened sample (method I).

size cannot be easily extended to the comparison between absorption spectra and size distribution measured from the TEM images. The absorption band edge of nonspherical semiconductor nanoparticles such as nanorods is mainly determined by the particle thickness,[25–27] that is, the direction of highest confinement. For different symmetries and geometries particle thickness may not be accurately measured by electron microscopy.

In conclusion, combining the information from PLE, size-selective precipitation, and TEM, we attribute the different optical components to species of different size rather than of different geometry.

Mechanisms for the Formation of Multiple Species. We can imagine different mechanisms leading to a multimodal size distribution. Each of them would imply its own characteristic evolution of the new components, which can be compared to the observations reported above. We propose four possible mechanisms and discuss their main features and possible causes. In reality more than one mechanism could occur at the same time and simultaneously to the classical growth of particles. In Figure 7 we represent the evolutions that we expect for each case, indicating each component with a stick. This scheme implicitly assumes that the horizontal axis represents both peak wavelength and particle size. This is justified by the quantum confinement, that is, the correlation between spectral energy and particle thickness.

The mechanisms we propose are the following.

(1) A secondary nucleation event during the growth stage: it would be characterized by a component appearing from the high energy side, having a faster red shift than the main component. In the three preparations, the high energy component does not move faster than the others or does not move at all: this mechanism can be ruled out for all the

(24) Flügge, S. *Practical Quantum Mechanics*, 2nd ed.; Springer: Berlin, 1994; p 48.

(25) Li, L. S.; Hu, J. T.; Yang, W. D.; Alivisatos, A. P. *Nano Lett.* **2001**, *1*, 349.

(26) Katz, D.; Wizansky, T.; Millo, O.; Rothenberg, E.; Mokari, T.; Banin, U. *Phys. Rev. Lett.* **2002**, *89*, 086801.

(27) Shabaev, A.; Efros, A. L. *Nano Lett.* **2004**, *4*, 1821.

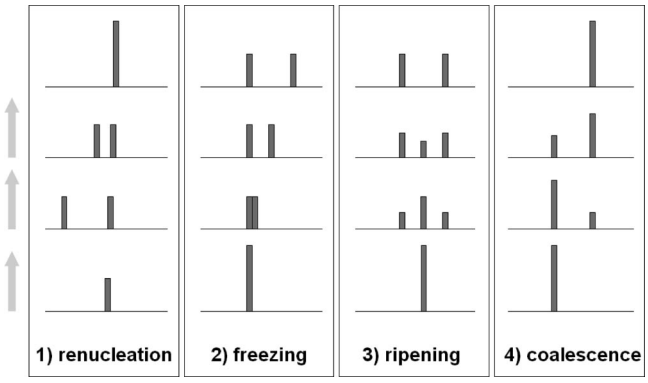

Figure 7. Scheme summarizing the spectral evolution for the four possible mechanisms (1–4) proposed in the text. We represent each component as a stick on a base corresponding to the wavelength axis, with a length proportional to the concentration, so that the bar patterns correspond to PL emission band patterns. From the bottom are reported stepwise the evolving situations for each of the mechanisms.

systems presented above. We actually did observe a clear instance of this mechanism with reaction II if we added octadecene during the growth stage (see Supporting Information S2). Interestingly, we observed no secondary nucleation if instead we added squalane, a branched alkane. This suggests that in method II nucleation is triggered by a chemical reaction of Se with the olefin, rather than just Se solubilization as argued by Cao et al.[20]

(2) Some of the particles stop growing: the number and the size of these "frozen" particles remain the same. New components at fixed intensity should be left uncovered on the high energy side, while the lowest energy component moves toward the red. The reason for the interrupted growth would be either that some particularly stable closed shell structures form or that a surface passivation occurs. This mechanism is unlikely for our cases. In Figure 8 we report in situ absorption measurements during the growth for preparations I and II. We see that in case I component B develops when A is already far enough on the red. In case II, component A is decreasing rather than shifting; however, B should already appear as a shoulder of A if it were present from the beginning. Also, with the emissions in Figure 3, we see a clear growth of the B component at short wavelength without a remarkable shift of the central peak.

(3) Ripening to stable particles of different shape and/or size: after the main peak stops red shifting, new peaks at fixed wavelength and increasing intensity should become obvious on both sides of the main peak. This mechanism is not contradicted by the behavior observed with method I. A correct evaluation should also consider intensities and cannot be done on the spectra of Figure 1, which have been recorded from a washed solution and normalized. There, one could only estimate relative variations among the different components. In situ absorption measurements during growth directly show absolute changes. In Figure 8I it is clear that component B develops on top of the increasing baseline and well after A has passed at its wavelength. Other components developing on the red side of A are not obvious; however, excitation-dependent emissions in Figure 4 reveal that indeed such components may be present, even if masked by more luminescent particles. On the other hand, the absence of a distinct peak for the large particles developing at the expense of the small ones does not exclude that they are present but only that their geometry is not well-defined. Indeed, TEM pictures show the effects of a coarsening process, with the more stable facets remaining after equilibration between different particles. Method III shows a similar sequence and arrangement with the components A, B, and C; thus, the mechanism seems likely as well. Finally, this mechanism also explains well the evolution with method II, reported in Figure 8II), in spite of the broad peaks. Although the evolution resembles an Ostwald ripening, we can see two components emerging at the extremes of the broadened central band. The spectra at room temperature show these components better (Figure 2).

(4) Particle aggregation and coalescence into larger ones: a new peak appears on the red side of the main one. The intensity of the low energy component increases at the expense of that of the high energy component. This could be what happens with component B in favor of component C in Figure 1, although it is difficult to establish that B does not broaden or disappear among further components. In the case of method III (Figure 3), this mechanism seems to describe well the growth of component C. With the spectra of method II, it is more difficult to find evidence.

Occasionally, we had evidence of the aggregation of the smallest particles during the size-selective precipitation, probably as a result of aging of the precipitate in methanol. In the example reported in Figure 9, we show emission spectra of a starting ripened sample and fractions precipitated out of it. The emission of the first fraction p1 spans to an even longer wavelength than does that of the initial sample. Some intensity is surprisingly present at a wavelength of 500 nm and less (note that a low-energy pass filter cuts the excitation and all wavelengths below 480 nm). This suggests that also very small particles have been precipitated out and then redissolved in toluene. Fraction s1]p2 is precipitated from s1, the supernatant of p1, and gives only the narrow band component 630 nm. TEM image reveals that this fraction actually consists of rice-like particles, with an XRD pattern (not shown) typical of a ZB structure. Probably the prolonged presence of methanol in solution promotes the attachment of two small particles into a rod-like structure of aspect ratio of about 2:1. This suggests that the intensity at 500 nm for p1 comes from small particles that aggregated without merging completely; once the precipitate is dissolved in toluene, they separate again. The remaining supernatant solution (s1]s2) has a slightly red-shifted spectrum compared to the initial one, likely because of fusion of the smallest particles. Elongated particles are usually considered to be wurtzite or wurtzite−ZB mixtures.[28] However, Li et al. have found the growth of ZB-stacked rods from CdSe dots in their controlled Ostwald ripening.[29] Wang et al. found a solvothermal route to obtain fully ZB CdSe rods, and they showed evidence for an oriented attachment mechanism.[30] In our case, an oriented attachment mechanism is also likely,

(28) Manna, L.; Scher, E. C.; Alivisatos, A. P. *J. Am. Chem. Soc.* **2000**, *122*, 12700.
(29) Li, R.; Luo, Z.; Papadimitrakopoulos, F. *J. Am. Chem. Soc.* **2006**, *128*, 6280.
(30) Wang, Q.; Pan, D.; Jiang, S.; Ji, X.; An, L.; Jiang, B. *J. Cryst. Growth* **2006**, *286*, 83.

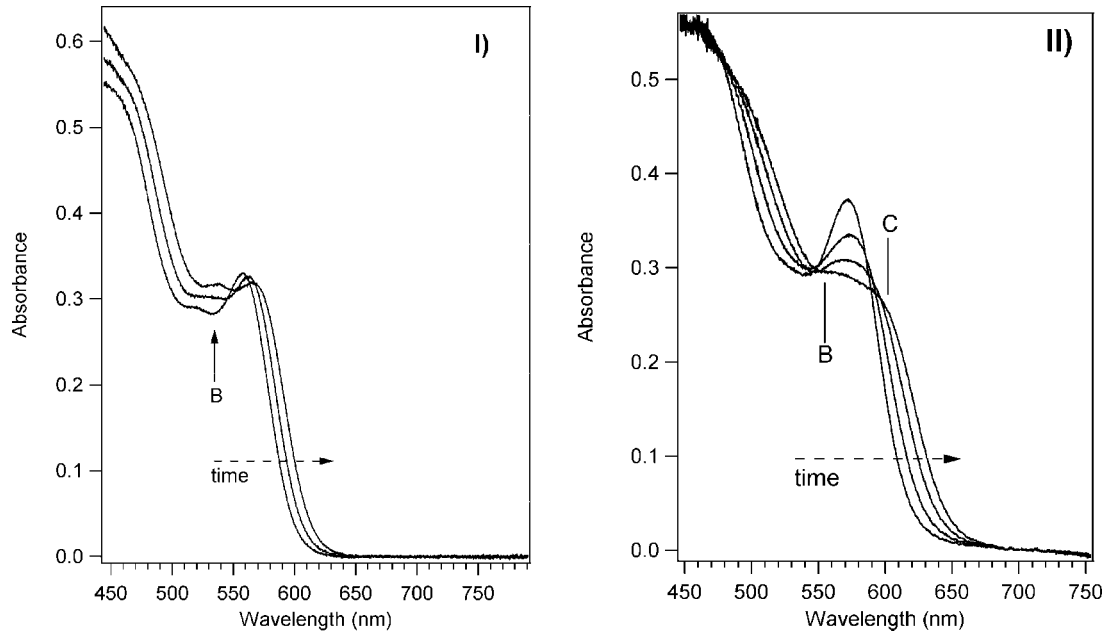

Figure 8. Overlapped absorption spectra taken in situ during preparations I and II at the moments when the new components become visible.

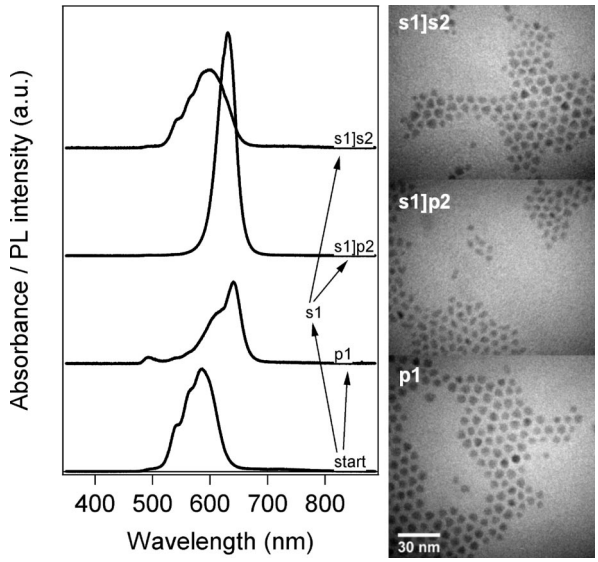

Figure 9. Emission spectra and TEM of the precipitated fraction of a ripened sample (method I).

possibly favored by the presence on the nanoparticles of facets assisting the assembly.

The existence of oriented attachment at room temperature supports the hypothesis that a similar process takes part also in the evolutions observed at high temperature. We can conclude that both mechanisms 3 and 4 appear to play a role in all three of the evolutions that we observed.

Mechanism 3 is also the one which best explains the polyhedral shapes observed in TEM images of the sample. These shapes result from the selective removal of weakly coordinated surface Cd and Se atoms, which leaves more stable flat crystal faces. The factors usually constraining the growth and ripening to spherical shapes, such as strong surface tension, may be relatively relaxed in our conditions.

Evidence for mechanism 4 is also strong: component C developing after B and elongated particles. In addition, using sizing equations,[31] we found that the wavelengths of the two remaining components often correspond to diameters having a ratio of 1.21–1.27. This ratio is close to the factor $2^{1/3}$, which is the one between the diameters of two spheres having volumes 2:1. This should be the case if the larger particle came from atom rearrangement into a more spherical shape after the two smaller particles fused together. Atom rearrangements have been proven in a few cases, for example, ZB to W transitions in nanowires assembled from ZB CdTe nanoparticles[32] or improved crystallization induced by water adsorption on ZnS at room temperature.[33]

All evolutions could be explained by the following scheme: at the end of the reactive growth regime, particle etching takes place, leading to faceted crystals of quite defined geometries and sizes. This process produces the planar surfaces where particles can attach to each other. Faceted crystals then start to fuse together and form larger particles, which rearrange into stable forms. Interestingly, oriented attachment has been often been found associated to Ostwald ripening.[15]

As suggested by an anonymous referee, we have attempted an estimation of the relative concentrations of the species A, B, and C as a function of heating time (see Supporting Information S3). We indeed find evolutions that qualitatively agree with a mechanism like A → B (etching); 2B → C (aggregation).

Chemical Conditions. Cho et al.[14] have found that PbSe NCs aged in air eventually attach to form nanowires. This suggests that geometric conditions may not be sufficient for

(31) Yu, W. W.; Qu, L. H.; Guo, W. Z.; Peng, X. G. *Chem. Mater.* **2003**, *15*, 2854.
(32) Tang, Z. Y.; Kotov, N. A.; Giersig, M. *Science* **2002**, *297*, 237.
(33) Zhang, H. Z.; Gilbert, B.; Huang, F.; Banfield, J. F. *Nature* **2003**, *424*, 1025.
(34) Li, R.; Lee, J.; Yang, B.; Horspool, D. N.; Aindow, M.; Papadimitrakopoulos, F. *J. Am. Chem. Soc.* **2005**, *127*, 2524.
(35) Nose, K.; Fujita, H.; Omata, T.; Otsuka-Yao-Matsuo, S.; Nakamura, H.; Maeda, H. *J. Lumin.* **2007**, *126*, 21.

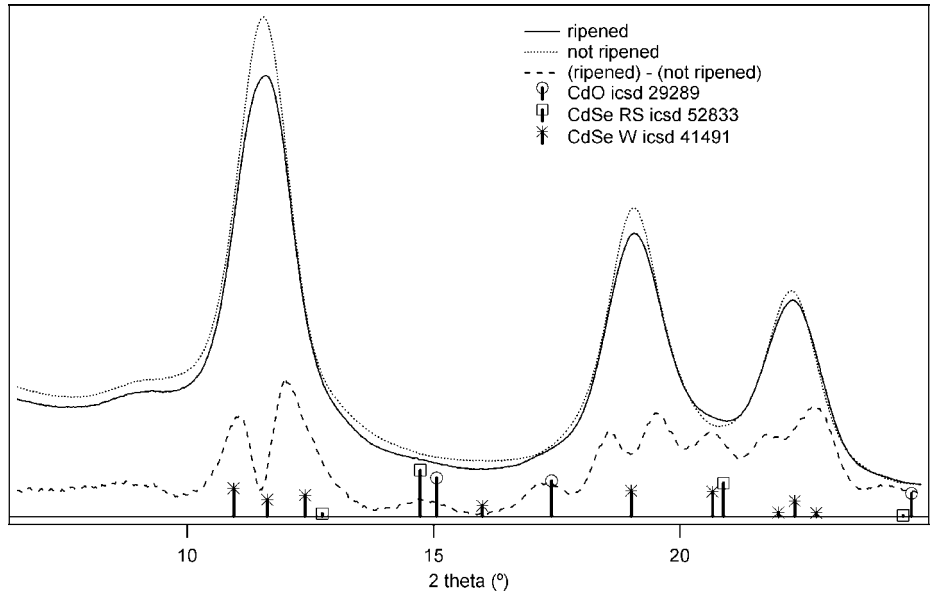

Figure 10. XRD patterns of a ripened and not ripened ZB sample and their difference. The reference patterns for CdO, W, and rock-salt CdSe are also shown. Patterns without normalization, vertically shifted for clarity.

the self-assembly process leading to particle coalescence. Possibly surface or ligand modifications are also required.

The mechanism we suggest here starts with a slow ripening regime. A detailed description of a faceted etching process of CdSe NCs has been given by Li et al.[34] They used a 3-amino-1-propanol/water medium at 80 °C in the presence of oxygen. Although in their conditions they did not observe the development of multimodal distributions, the basic process could present analogies to our case. They proved that dissolved oxygen is responsible for the etching, while water, by forming surface oxides/hydroxydes layers, moderates the etching rate and favors the surface reconstruction.

Traces of dissolved oxygen are likely in our system. Although our reactions were always performed under an inert gas stream, all preliminary manipulations were carried out in air, and we did not operate any specific O_2 removal. Additional oxygen was introduced while sampling during growth.

Also, water is present in the system, as our method implied starting either from hydrated Cd acetate or from the reaction of CdO with a fatty acid, with elimination of water:

$$CdO + 2R{-}COOH \rightarrow Cd(R{-}CO_2)_2 + H_2O$$

At the reaction temperature, water can be also produced by the condensation of excess fatty acid to give an anhydride:

$$2R{-}COOH \rightarrow R{-}COOCO{-}R + H_2O$$

In the case of preparation I, ODA may react with either a carboxylic or a phosphonic acid, to give an amide:

$$R{-}COOH + R'{-}NH_2 \rightarrow R{-}CONH{-}R' + H_2O$$

$$R{-}PO(OH)_2 + R'{-}NH_2 \rightarrow R{-}PO(OH)NH{-}R' + H_2O$$

If we take this neutralization reaction into account, we can infer that in all three preparations presented here we do not work with a large excess of alkyl amine, which is an additive widely used to favor high luminescence and narrow size distributions.[1] Its action is still not fully understood, but it is possible that with its basic character this molecule may interfere with the activity of the water traces, which is undesired when the goal is a monodisperse ensemble of dots. Indeed, luminescence has been recently correlated with the amine basicity.[35]

Interaction with the polar functions of the surfactants could delay water removal, which otherwise should be fast above 200 °C. Oxygen and water, either not fully removed by heating or formed by reactant decomposition, should trigger the particle etching and aggregation.

Li et al.[34] suggested the following reaction between CdSe and oxygen:

$$CdSe + \frac{3}{2}O_2 \rightarrow CdO + Se_2O$$

with the produced oxides dissolved by the species in solution. In our conditions we may also have

$$CdSe + O_2 + 2R{-}COO^- \rightarrow Cd(R{-}COO)_2 + Se_2O$$

But at our ripening temperature, also hydrolysis and dissolution reactions should become significant

$$CdSe + H_2O \rightarrow CdO + H_2Se$$

$$CdO + H_2O + 2R{-}COO^- \rightarrow Cd(R{-}COO)_2 + 2OH^-$$

The rate of these side reactions should be small compared to the reactive CdSe growth from the monomers as long as these are available. Afterward, when reactive growth has settled, reaction with water and oxygen competes with Ostwald ripening (which instead should only involve soluble species). The reactivity should be higher for not well-coordinated surface atoms. Atoms belonging to flat, reconstructed surfaces will offer superior resistance to etching. CdO formation may provide a passivation for such relatively stable sites. As a result of this, we observe characteristic peaks appearing (component B), of thinner CdSe species.

Indeed, we found traces of CdO in ripened samples by XRD, reported in Figure 10. A difference spectrum with a

not ripened ZB sample helps to detect changes. The wings on the sides of the main ZB reflex are simply due to the different peak widths, that is, different particle sizes. The remaining peaks are localized at 14.8, 17.3, 20.6, and 24.2°. Only the 20.6° peak can belong to a CdSe phase; it is probably the wurtzite (103). This would confirm that heat treatment induces a limited phase switch from ZB to W, in agreement with what may be suggested by Figure 4, with smaller splitting between the first two exciton bands for the most red-shifted PLE spectra. The other three fit the ICSD (Inorganic Crystal Structure Database) file 29289 of rock salt CdO fairly well, having peaks at 2θ of 15.0, 17.4, and 24.7°, corresponding to the (111), (200), and (220) reflexes. The systematically smaller angle suggests a certain strain for this phase. From the relative intensity of these peaks, we estimate less than 2% of Cd in the form of ordered oxide domains. CdO traces are found in comparable amounts in different fractions separated by size-selective precipitation; it is thus likely that it is part of all the NCs. The strain suggests its localization on the surface. CdO seems to be participating in this surface reconstruction in the form of a tiny layer, occasionally as few monolayers (as required in order to observe an XRD pattern). We were not able to distinguish the CdO layer between the CdSe core and the organic capping by X-ray photoemission spectroscopy (XPS). The signals of the Cd 3d, O 1s, and O 2p levels were sharp monocomponent peaks, possibly because of the vicinity of the chemical shifts to the more abundant CdSe and $R-COO^-$ species. We cannot remark on the differences with samples that were not etched. We also did not note any trace of SeO_2 in the Se 2p spectra.

The presence of CdO can be directly attributed to the etching process suggested above or to an oxidation of the dried sample in air, before XRD measurement. Although we cannot rule out this second possibility, in both cases its presence suggests a depletion of surface ligands. Surfaces partially covered by CdO could be differently terminated (e.g., OH groups) and thus no more strongly attached by the polar or charged ligand head. On the other hand, formation of CdO by oxidation in air is in itself evidence that surfaces have been depleted of organic ligands and made accessible to oxygen before exposure to air. Also, this case may well be an effect of the presence of water or oxygen, which would react with the ligands.

Depletion of surface ligands, regardless whether cause or consequence of the CdO formation, is expected to promote assembly and coalescence of particles in the organic medium.

In summary, our results show that the presence of water and/or oxygen during the high temperature ripening of colloidal CdSe spherical particles favors the etching into faceted shapes possibly covered by oxide layers. We have evidence that such particles are able to undergo oriented attachment to produce elongated shapes, which may eventually rearrange to form larger particles.

Note that this oriented attachment mechanism differs from the one suggested by Zhang et al. [18] and mentioned in the introduction. Reactive growth may well imply coalescence of small clusters, but this process becomes less relevant with increasing particle size. The coalescence involving large particles must be of a different nature and only occurs when specific chemical conditions are met. It is remarkable that in both cases sharp size distributions are the result.

Conclusions

In this paper we have presented three different synthetic methods for the preparation of CdSe colloidal nanoparticles leading to unusual spectra when carried out beyond the stage of reactive growth. Instead of the broadening expected with an Ostwald ripening, we observed the development of complex spectral patterns. We have shown that the spectra result from the overlapping of several distinct components, which correspond to different kinds of nanoparticles coexisting in solution. Although several polyhedral shapes are present, the main spectral difference appears to be due to different sizes. We explain the generation of the different species with a mechanism implying a controlled etching of the initially spherical particles and a subsequent aggregation and fusion of small into larger particles. We suggest that the presence of water and oxygen in the chemical equlibria can favor the evolutions we observed.

We hope these findings will stimulate a closer inspection of the different possible interparticle equilibria in the growth stage commonly referred to as Ostwald ripening. A better understanding of such processes may lead to simple methods to control the size distribution and the geometrical shape of colloidal CdSe nanoparticles.

Acknowledgment. The authors thank Dr. Francois Patthey for the XPS measurements and the Swiss National Science Foundation (NCCR "Quantum Photonics") for financial support.

Supporting Information Available: TEM images of size-selected ripened NCs and absorption spectra showing the effect of octadecene addition during method II (PDF). This material is available free of charge via the Internet at http://pubs.acs.org.

CM071439U